J Solid State Electrochem (2011) 15:737–745
DOI 10.1007/s10008-010-1146-1

ORIGINAL PAPER

Underpotential deposition of cobalt onto polycrystalline platinum

Luis H. Mendoza-Huizar · Clara H. Rios-Reyes

Received: 1 December 2009 / Revised: 28 June 2010 / Accepted: 12 July 2010 / Published online: 24 July 2010

Abstract An electrochemical study of cobalt electrodeposition onto a polycrystalline platinum electrode from an aqueous solution (10^{-2} M $CoCl_2$+1 M NH_4Cl (pH 9.5)) was carried out through cyclic voltammetry and potential step techniques. Analysis of the voltammetric data clearly showed that a cobalt adlayer is formed during the application of potential in the underpotential deposition (upd) region. Formation of this cobalt adlayer involved the simultaneous presence of both adsorption and 2D nucleation processes. Cobalt adlayers obtained by linear voltammetry in upd region were analyzed employing diffuse reflectance spectroscopy (DRS). By using theoretical quantum studies at PM6//HF/LANL1MB level, it was possible to assign the peaks obtained by DRS at 328 and 337 nm to the cobalt adsorption on Pt(111) and Pt(100), respectively, while the signals recorded at 355 and 362 nm were related with the clean platinum surfaces Pt(100) and Pt(111). Also, quantum calculations at the PM6 level indicated that the energy formation order is Co-Pt(100)> Co-Pt(111)>Co-Pt(110)>Co-Co(surface).

L. H. Mendoza-Huizar (✉) · C. H. Rios-Reyes
Centro de Investigaciones Químicas, Mineral de la Reforma,
Universidad Autónoma del Estado de Hidalgo,
Hidalgo, C.P. 42181, Mexico
e-mail: hhuizar@uaeh.edu.mx

C. H. Rios-Reyes
Departamento de Materiales,
Universidad Autónoma Metropolitana-Azcapotzalco,
Av. San Pablo 180, Col. Reynosa Tamaulipas,
C.P. 02200 México, D.F., Mexico

Keywords Cobalt · Platinum · Monolayer · Underpotential · PM6

Introduction

Co adlayers on Pt surfaces exhibit a strong magnetic anisotropy useful in the fabrication of magnetic storage devices [1–4]. This property has motivated the study of ordered and disordered overlayers of Co on Pt, due to their potential applications in the fabrication of electronic devices [4–10]. Most of these Co overlayers have been prepared employing molecular beam evaporation techniques [4, 11–13]. Although, it has been reported that the electrodeposition process allows getting overlayers of cobalt [14, 15], few studies have considered the electrodeposition as a way to obtain Co overlayers onto Pt [16–21]. The electrodeposition has the advantage to be itself an economic and simple technique, but it requires a very good knowledge of the nucleation and growth parameters to acquire deposits with reproducible properties. Moreover, a better understanding of the kinetic deposition phenomena will provide a better control of their magnetic and electronic properties. Albeit, the interest devoted to the fabrication of thin films of cobalt/platinum, up to our knowledge, there is not information regarding the kinetic details of the electrodeposition process of cobalt onto polycrystalline platinum surfaces. Therefore, in order to gain a deeper insight into this system, in the present paper, we report a study of the electrodeposition of cobalt onto polycrystalline platinum at underpotential conditions, by using cyclic voltammetry and chronoam-

perometry. Characterization techniques such as diffuse reflectance spectroscopy (DRS) and theoretical quantum studies were also employed during the study.

Methodology

Experimental

Cobalt electrodeposition on a platinum electrode was studied from an aqueous solution containing 10^{-2} M of $CoCl_2$ and 1 M NH_4CI, at pH 9.5 (adjusted with NaOH) at 25 °C. Under these conditions, the main chemical species of the Co (II) ion is the $[Co(NH_3)_5(H_2O)]^{2+}$ complex [22]. We verified the existence of $[Co(NH_3)_5(H_2O)]^{2+}$ complex, as predominant chemical species elaborating the corresponding Pourbaix's diagrams and the results obtained are completely coincident with those reported in literature [22]. The equilibrium potential in the $[Co(NH_3)_5(H_2O)]^{2+}/Co^0$ redox system has been determined as -0.786 vs SCE [22], (−0.741 V vs Ag/AgCl) agreeing with Eq. 1.

$$\left[Co(NH_3)_5(H_2O)\right]^{2+} + 2e \rightarrow Co^0 + 5NH_3 \quad (1)$$

All solutions were prepared using analytic grade reagents with ultra pure water (Millipore-Q system) and deoxygenated bubbling N_2 for 15 min before each experiment. The working electrode was a polycrystalline platinum rotating disk electrode tip provided by Radiometer Tacussel of 0.0314 cm^2; the exposed surface was polished to a mirror finish by using Alfa Aesar aluminum oxide and cleaned ultrasonically. A graphite bar with an exposed area bigger than the working electrode was used as a counter electrode. An Ag/AgCl electrode was used as the reference electrode, with all measured potentials referred to this scale. The electrochemical experiments were carried out in a BAS 100 W potentiostat–galvanostat connected to a personal computer running BAS100W software to allow the control of experiments and data acquisition. In order to verify the electrochemical behavior of the electrode in the electrodeposition bath, cyclic voltammetry study was performed within the 0.6 to −1.0 V potential range at different scan rates.

Theoretical

The cobalt adsorption process onto three monocrystalline platinum surfaces (100), (110), and (111) were analyzed. These platinum surfaces represent the principal crystallographic orientations for the face-centered cubic lattice of polycrystalline platinum [23]. Platinum surfaces were modeled employing a theoretical methodology reported previously [24] by means of finite cluster's size of 25, 13 and 22 atoms for the (100), (110), and (111) orientations, respectively, by using crystallographic parameters [25]. In all calculations, we performed restricted optimizations where the adsorption of cobalt atoms was optimized while the coordinates of surface atoms were fixed. In present work, we test the ability of the PM6 method [26] in combination with the HF/LANL1MB level [27] to predict the adsorption geometries of cobalt onto platinum and the optical band gaps of the Pt-Co system, respectively.

Computational resources

We employed a Beowulf cluster with 6 processors of 2.4 GHZ each one with a 1 GB of RAM for all calculations. These calculations were performed with the Package MOPAC2007 Linux version [28], Gaussian03W [29] and were visualized with a Winmostar graphical interface [30].

Results and discussion

Cyclic voltammetry study

Figure 1 shows the cyclic voltammogram obtained for the Pt/10^{-2} M $CoCl_2$+1 M NH_4CI system at pH=9.5 at 20 mVs^{-1} of scan rate. The potential scan started at 0.6 V in the negative potential direction up to −1.0 V, and then it was reversed to the starting potential. During the direct scan, it is possible to observe three peaks A, B, and C at the potential values of −0.120, −0.600, and −0.840 V, respectively. Note that peaks A and B appear at more positive potentials than −0.741 V, in the underpotential deposition (upd) zone of cobalt. It is important to note that the process associated to peak B starts at −0.450 V approximately, this potential value is similar to that found by Herrero et al. [17] when a cobalt adlayer is deposited on Pt(111) from 0.01 M

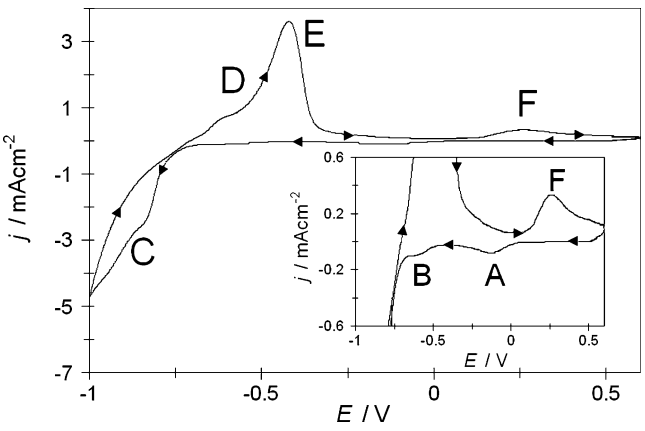

Fig. 1 Cyclic voltammogram obtained in the Pt/10^{-2} M $CoCl_2$+1 M NH_4Cl (pH 9.5) system. The potential scan was started at 0.600 V towards the negative direction with a potential scan rate of 20 mVs^{-1}. Arrows indicate the potential scan direction. Cathodic density current peaks (*a*, *b*, and *c*) and anodic peaks (*d*, *e*, and *f*) are also indicated

$CoCl_2$ in 0.1 M NaOH. In overpotential deposition (opd) conditions, the electrodeposition process begins at −0.741 V. This potential value suggests either a great affinity between the electrodeposited cobalt onto the platinum surface or an electrodeposition process on a cobalt monolayer. After peak C, observe the change of the slope in the voltammetric curve. This change may be related to hydrogen evolution since it is predominant in this zone. When the potential scan was inverted, a shoulder (D) and two anodic peaks, E and F, appeared at −0.610, −0.410, and 0.260 V, respectively. A comparison of the voltammogram showed in Fig. 1 with the voltammetric curve obtained from the system Pt/1 M NH_4CI system at pH= 9.5 at 20 mVs^{-1} is depicted in Fig. 2. From this figure, it is possible to conclude that peak A is due to the supporting electrolyte and peak B may be associated with cobalt reduction processes. Note that peak B is formed by two overlapped signals which may correspond either the formation of two cobalt submonolayers on the polycrystalline surface or well to a charge transfer process from Co(III) to Co(II). However, a transfer charge from Co(III) to Co(II) must be occurring at potentials values more positive than the considered at present work which implies that the formation of submonolayers is a more probable process. The slightly potential displacement may be caused by the different crystallographic orientations which are present on a polycrystalline surface. A typical behavior of an upd process is that the peak relevant associated to the upd process first appears in cyclic voltammetry at lower concentration of metallic ions. Then the peak increases with the metal ion concentration increasing before a full 2D coverage has been formed. In order to verify this behavior in our system, we carried out a set of cyclic voltammetries

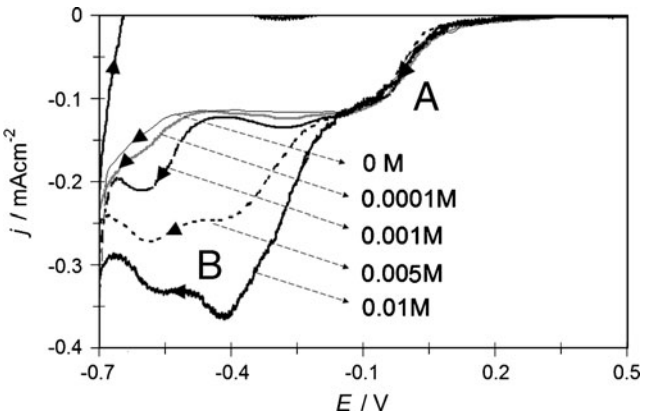

Fig. 2 Comparison of cyclic voltammetric curves obtained in the Pt/*x* M $CoCl_2$+1 M NH_4Cl (pH 9.5) system at different Co^{2+} concentrations (*x*=0, 0.0001, 0.001, 0.005, and 0.01 M) indicated in the figure. The potential scan was started at 0.600 V towards the negative direction to −800 mV with a potential scan rate of 20 mVs^{-1}. *Arrows* indicate the potential scan direction. Cathodic density current peaks (*a* and *b*) and anodic peaks (*d*, *e*, and *f*) are also indicated

employing different cobalt concentrations (0.0001, 0.001, 0.005, and 0.01 M). The results obtained in upd zone are showed in Fig. 2. Note that at lower cobalt concentration, it appears the peaks A and B. Peak A have been associated previously to the supporting electrolyte which remains practically constant while peak B associated to upd process is increasing with the cobalt concentration. Last result is typical of an upd process suggesting that peak B is due to the cobalt electrodeposition in underpotential conditions. Similar behavior has been reported during the upd processes of zinc on Pt(111) [31] and Pb on Pt(100) [32]. For the case of anodic signals D, E, and F, there are several interpretations about cobalt oxidation mechanism. Thus, the shoulder D has been associated to the dissolution of the hydrogen-rich cobalt phase [33], peak E to the cobalt dissolution of cobalt previously deposited in opd conditions while F was related to the oxidative dissolution of the electrodeposited cobalt in upd conditions [14]. However, it is important to mention that an exhaustive study to identify the dissolution mechanism it was not done. Recently, Grujicic et al. [34] have reported that the overall cobalt oxidation mechanism, involves hydroxide forms either as an intermediate or as a final product of oxidation. Under these considerations, and taking into account the Pourbaix's diagram [35], cobalt electrodeposited is passivated in aqueous solutions by forming a hydrated cobalt oxide layer, $Co(OH)_2$, according to a hydrolytic reaction (2):

$$Co + 2OH^- \rightarrow Co(OH)_2 + 2e \quad (2)$$

Thus, the reaction mechanism at basic conditions involves the presence of free ammonia for reactions, in our conditions the proposed mechanism for peaks D and E is:

$$Co(OH)_2 + 2NH_4Cl \rightarrow CoCl^+ + Cl^- + 2NH_3 \cdot H_2O \quad (3)$$

$$CoCl^+ + Cl^- + 2NH_3 \cdot H_2O \rightarrow Co(NH_3)_2^{2+} + 2Cl^- + 2H_2O \quad (4)$$

$$Co(OH)_2 + 2NH_4Cl + 2NH_3 \cdot H_2O \rightarrow Co(NH_3)_2^{2+} + 2Cl^- + 2H_2O \quad (5)$$

It is important to mention that at the same potential range in where the anodic signal F was detected, Herrero et al. [17] have reported evidences of the oxidation of $Co(OH)_2$ to the $Co(OH)_3$ while Vaskelis et al. [36] found an oxidation process of Co(II)amine complex to the Co(III)amine complex. In order to analyze if peak F corresponds to an oxidation process of Co(II)amine complex to the Co(III) amine complex we carried out a set of linear voltammetries at four baths with different cobalt concentrations (0.0001, 0.001, 0.005, and 0.01 M) starting the oxidation process at 0 mV toward anodic direction to 600 mV. Note that under these experimental conditions, Co^0 is not present. A

comparison of a linear voltammetry with a cyclic voltammetry for the bath with 0.01 M of cobalt concentration is depicted in Fig. 3. Note that when the scan is carried out from 0 to 600 mV in anodic direction peak F was not recorded, the same behavior was obtained for different cobalt concentrations indicating that an oxidation of Co(II) amine complex to the Co(III)amine complex was not present. However, according with Eq. 2, cobalt electrodeposited in aqueous bath, inclusive in upd conditions, might be passivated by forming $Co(OH)_2$ and this situation might cause the presence of peak F. In order to confirm the correspondence among peaks A, B and C with shoulder D, and between peaks E and F, we performed cyclic voltammograms at different inversion potentials at a constant scan rate (20 mVs^{-1}) as is shown in Fig. 4. In the upd zone (E≥0.741 V), see inset in Fig. 4, two main current density peaks (A and B) were recorded during the direct scanning. At the inversion potential value of −0.300 V, Fig. 4b, the peak A is fully formed; at this point, we inverted the scan and a clear anodic signal was not detected. When more negative potentials were reached, Fig. 4d-f (peak B), an anodic signal at approximately 0.260 V (peak F) was recorded. The current density of peak F was increased in function of inversion potential. These results suggest that the anodic peak F is due to the dissolution of cobalt deposited in upd conditions (peak B). When the inversion potential was lower than −0.800 V, we detected a wide anodic peak at −0.550 V which can be related to the dissolution of cobalt deposited in peak C following the Eqs. 3, 4, 5. At more negative potentials, a displacement of these signals to the anodic direction was observed. In all cases, the voltammetric curves in Fig. 4 were compared with their equivalent curves in the supporting electrolyte and the

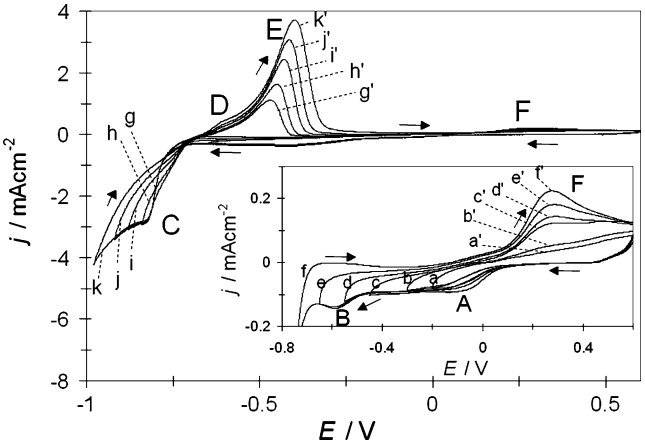

Fig. 4 Cyclic voltammograms obtained in the Pt/10^{-2} M $CoCl_2$+1 M NH_4Cl (pH 9.5) system at different inversion potentials of (*a-a′*) −0.200 V, (*b-b′*) −0.300 V, (*c-c′*) −0.450 V, (*d-d′*) −0.550 V, (*e-e′*) −0.650 V (*f-f′*), −0.750 V (*g-g′*), −0.800 V, (*h-h′*) −0.840 V, (*i-i′*) −0.880 V, (*j-j′*) −0.920 V, and (*k-k′*) −0.980 V. In all cases, the potential scan started at 0.600 V towards the negative direction with a potential scan rate of 20 mVs^{-1}. *Arrows* indicate the potential scan direction. Cathodic current density peaks (*a*, *b*, and *c*) and anodic peaks (*d*, *e*, and *f*) are also indicated

general behavior was as shown in Fig. 2. Last results suggest the presence of an upd cobalt process on the polycrystalline platinum electrode.

In order to analyze the influence of the scan rate in the cobalt electrodeposition process on platinum, we carried out a voltammetric study at different scan rates. The cyclic voltammograms are shown in Fig. 5. Note that the current density associated to each peak depends on the scan rate. The potential values associated to peaks A and B exhibits a small variation in each case. During the sweep in the positive direction, peak E increases faster with the scan rate in

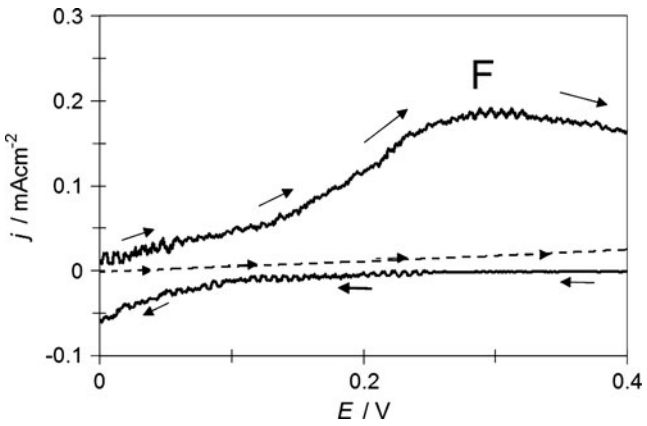

Fig. 3 Comparison of two voltammetric curves obtained from the Pt/10^{-2} M $CoCl_2$+1 M NH_4Cl (pH 9.5) system. **a** Cyclic voltammogram obtained when the potential scan was started at 0.600 V towards the negative direction to −1.000 V and reverted to 0.600 V (*solid line*), **b** linear voltammogram obtained when the scan potential was started at 0 mV toward anodic direction to 600 mV (*broken line*). For sake of clarity, in the figure is only depicted the potential range 0–0.4 V

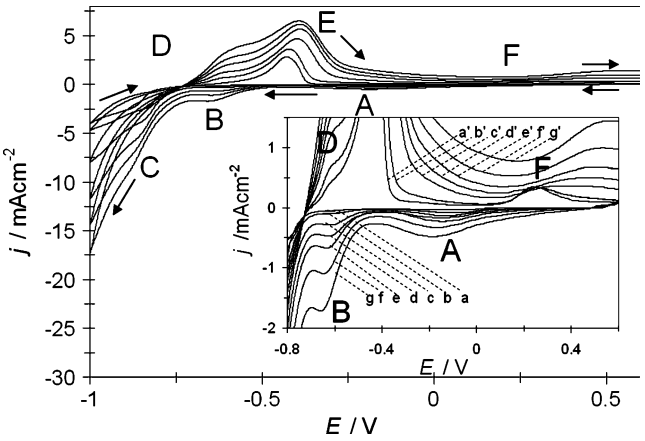

Fig. 5 Cyclic voltammograms obtained in the Pt/10^{-2} M $CoCl_2$+1 M NH_4Cl (pH 9.5) system at different scan potential rates of (*a-a′*) 10, (*b-b′*) 20, (*c-c′*) 60, (*d-d′*) 100, (*e-e′*) 150, (*f-f′*) 250, and (*g-g′*) 400 mVs^{-1}. In all cases, the potential scan was started at 0.600 V towards the negative direction. *Arrows* indicate the potential scan direction. Cathodic density current peaks (*a*, *b*, and *c*) and anodic peaks (*d*, *e*, and *f*) are also indicated

comparison with peaks D and F, indicating that a predominant phase is being deposited during the direct scan.

In order to determine the type of limiting control for the opd process, the current density (j_p) value associated with peak C was plotted as a function of $v^{1/2}$ (v = potential scan rate). The result is shown in Fig. 6. Therein, we may observe a linear relationship, indicating a diffusion control for the opd process according with the Berzins-Delahay equation [37, 38]. From the plot, it was possible to calculate a diffusion coefficient value of 1.8×10^{-6} cm/s^{-1} which is close to the experimental value reported in literature [22].

Kinetic of cobalt upd adlayer

Detailed information about the electrocrystallization process can be obtained from potentiostatic deposition. Figure 7 shows a set of current transients recorded at different potentials from 10^{-2} M of $CoCl_2$ and 1 M NH_4CI at pH 9.5. In all cases, the experiments involved the application of an initial potential of 0.600 V on the platinum electrode surface. Under this potential condition, cobalt deposition had not started yet, as could be easily noted from the previous voltammetric study. After application of this initial potential, a second negative potential step was applied to the electrode surface for 32 s within the range of −0.400 to 0.700 V every 0.050 V. It should be noted that these potential values are in the cobalt upd region. The shape of these transients is quite similar to those reported by Hozle et al. [39] and Mendoza-Huizar et al. [14]. The theoretical description of similar potentiostatic current transients as shown in Fig. 7 has been predicted adequately by [14]:

$$j_{total}(t) = j_{ad}(t) + j_{2Di-dc}(t) \quad (6)$$

where

$$j_{ad}(t) = k_1 e^{-k_2 t} \quad (7)$$

and

$$j_{2Di-dc}(t) = k_3 e^{-k_4 t} \quad (8)$$

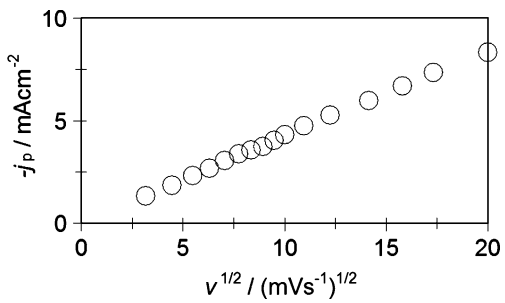

Fig. 6 Plot of the experimental cathodic peak current density (j_p) as a function of scan rate ($v^{1/2}$) for Peak C (see Fig. 1)

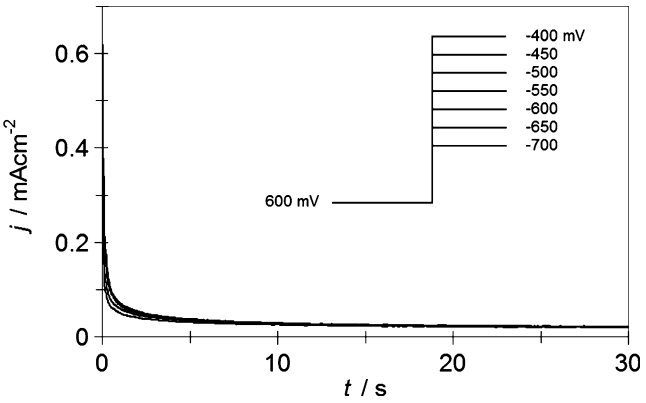

Fig. 7 Set of experimental current transients recorded during the upd process in the Pt/10^{-2} M $CoCl_2$+1 M NH_4Cl (pH 9.5) system. In all cases, the starting potential of 0.600 V was applied to the platinum electrode surface and t=32 s

$j_{ad}(t)$ is the current density for a Langmuir type adsorption–desorption process and $j_{2Di}(t)$ is the current density associated to an instantaneous two-dimensional nucleation mechanism. $k_1=k_2Q_{ads}$, and Q_{ads} is the charge density due to the adsorption process. The potential dependence of k_2 is assumed to obey the Butler–Volmer relation. Then, the adsorption of metal ions associated with the charge transfer is given by Eq. 14 in Ref. [37]. $k_3 = q_{mon}\pi S^2 D$, $k_4 = \pi S^2 DN_0$, In these equations, q_{mon} is the charge density associated with formation of the monolayer, S is a constant controlled by the potential, D is the diffusion coefficient of the metal ion, and N_0 is the density number of active sites. Note that $k_3=k_4Q_{nucl}$ and Q_{nucl} is the charge density due to the 2D nucleation process. Figure 8 shows a comparison of the experimental current transients obtained during cobalt upd and that generated theoretically by nonlinear fitting of Eq. 6 to the experimental data. From the figure, it becomes clear that the nucleation–adsorption

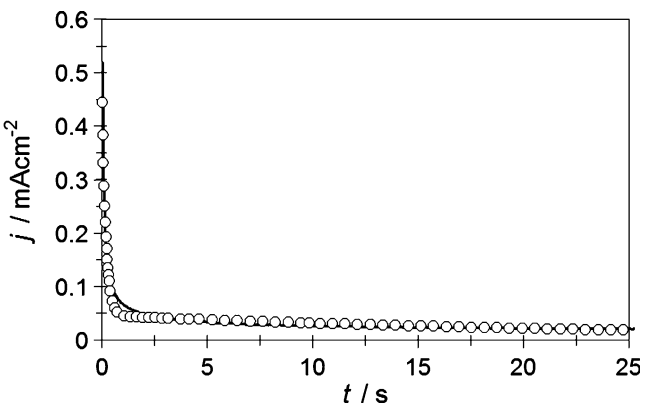

Fig. 8 Comparison of an experimental current density transient (—) recorded during cobalt electrodeposition at −650 mV V onto a polycrystalline platinum from an aqueous 10^{-2} M $CoCl_2$+1 M NH_4Cl (pH 9.5) solution and a theoretical transient (*open circles*) obtained by non-linear fit of Eq. 6

model can adequately describe the whole experimental current transient. Table 1 shows the parameters pertaining to Eq. 6 that best fitted the experimental transients. It is interesting to observe that the contribution due to the nucleation process is 93% indicating that under our experimental conditions the 2D nucleation process is favored.

Diffuse reflectance at different potentials

DRS has established its effectiveness in qualitative and semi-quantitative analysis as a technology for nondestructive characterization of the composition of materials based on the interaction of visible infrared light (electromagnetic energy) with matter [40]. The diffusely reflected radiation collected and detected by the detector is converted into a spectrum that is similar to absorbance spectrum in transmittance spectrometry; where peaks are increased without modify the positions of these in DRS [40]. Reflectance technique has been successfully used in the study of optical properties of nanostructured metal films such as platinum, gold and silver [41] and the underpotential deposition of Pb on gold [42]. Figure 9 shows diffuse reflectance spectra in UV zone (DRS-UV) of deposits obtained at 100 mVs^{-1} of scan rate with linear voltammetry at different final potentials located in upd zone; the initial potential value was 600 mV where no cobalt electrodeposition has started yet. It is important to mention that, in all cases, DRS signals were only detected in the 327–386 nm range. The DRS-UV for clean polycrystalline platinum is shown in Fig. 9a where the presence of two peaks at 355 and 362 nm, can be related to two principal faces in the polycrystalline surface. Figure 9b shows the results obtained when DRS signals were obtained from the supporting electrolyte, a main signals were detected at 342, 356, 362, and 383 nm. The signals at 356 and 362 nm may correspond to clean polycrystalline platinum, while the signals recorded at 342 and 383 nm may be caused by the adsorption of ions which may be Cl^{-}, NH_4^{+}, H^{+}, or O^{-2}. DRS-UV for the deposit of cobalt obtained at −550 mV, Fig. 9c, shows three main peaks at 337, 361, and 383 nm. The peak at 361 nm is probably due to the polycrystalline platinum while peak 383 nm is caused by anion adsorption. The peak recorded at 337 may be

Table 1 Best fit parameters obtained from non-linear adjustment of Eq. 6 to the experimental current density transient recorded during cobalt upd onto platinum electrode (see Fig. 8)

E/mV	k_1/mAcm^{-2}	k_2/s^{-1}	k_3/mAcm^{-2}	k_4/s^{-1}	%Q_{ads}	% Q_{2D}
650 mV	0.471	5.537	0.046	0.038	6.51	93.49

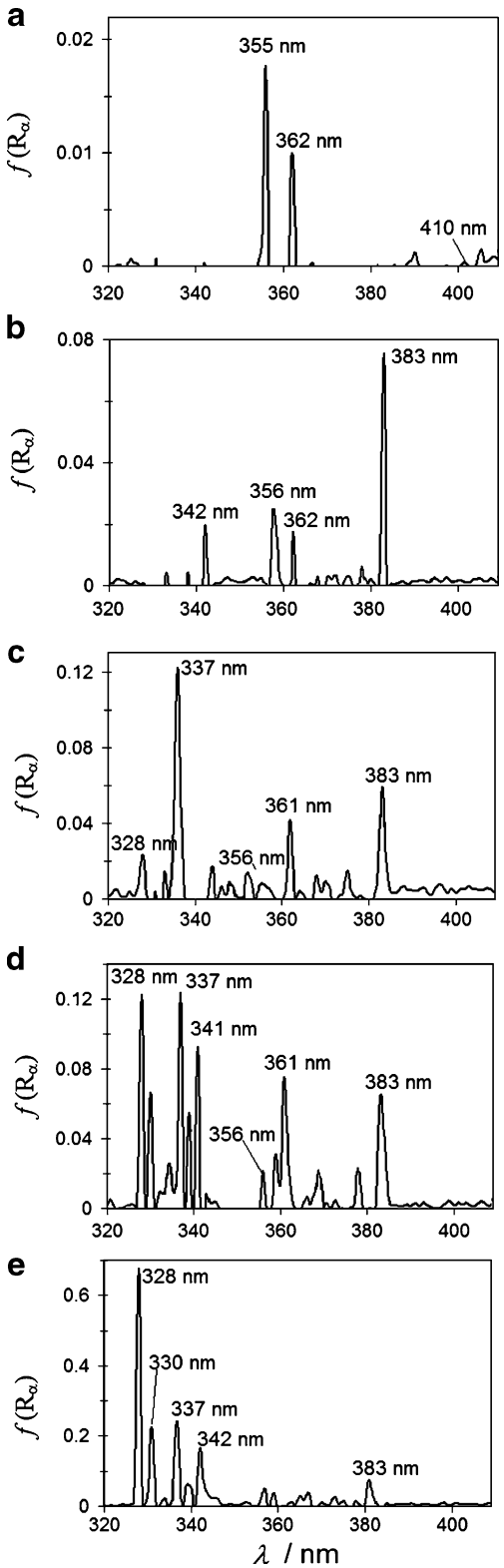

Fig. 9 Diffuse reflectance spectra in Ultraviolet zone of cobalt electrodeposits obtained on polycrystalline platinum by linear voltammetry at different final potentials. **a** Clean polycrystalline platinum, **b** from supporting electrolyte on polycrystalline platinum, **c** −0.550, **d** −0.600, and **e** −0.700, supported on KBr

associated with a cobalt submonolayer deposited on the polycrystalline surface. At −600 mV, Fig. 9d, six main peaks at 328, 337, 341, 356, 361, and 383 nm were observed. It is probable that the additional peak at 328 nm is due to the formation of a new cobalt submonolayer on a different crystallographic orientation. The deposit obtained at −700 mV, Fig. 9e, showed five peaks at 328, 330, 337, 342, and 383 nm. It is interesting to note that at this last potential value, the peaks corresponding to the clean platinum surface are smaller in comparison with the new peaks, which suggests that the platinum surface is being covered with cobalt at different crystallographic orientations.

Theoretical quantum study

In order to establish the correspondence of the peaks observed in the DRS-UV spectra with the adsorption of cobalt onto platinum surfaces; we performed a theoretical quantum study to calculate the optical band gaps associated to the models shown in Fig. 10. A disadvantage of the theoretical quantum methods to simulate macroscopic systems (surfaces) is the current computational limit, in particular when ab initio calculations are considered. Therefore, if one considers a solid as a big molecule and the fact that several processes, such as single atom/molecule adsorption or single impurities, are localized phenomena, it becomes clear that a cluster model may be a good starting point for a theoretical description of a superficial phenomenon. In such cluster approach, the surface may be simulated by using a small number of atoms. If we include more and more atoms, the description will become more accurate. However, the calculation time and the computer memory required increases quickly as the system grows, in particular when ab initio methods are used [43]. Recently, the semiempirical method PM6 developed by Stewart's group offers new possibilities to model solid state reactions in modest workstations [44]. Up to our knowledge, the PM6 method has not been applied in analyzing the adsorption process of cobalt on platinum. Thus, in the present work, we used the PM6 method in combination with the HF/LANL1MB [27] level, to predict the optical band gaps of the Co/Pt system. The HF/LANL1MB level was chosen after a previous calibration process (not shown here), since this level of theory proved to be adequate to predict adequately some experimental electronic properties such as the work function and the band gap value of clean platinum surface. Fig. 10a-d shows the optimized structures of one cobalt atom adsorbed on three different Platinum surfaces such as (100), (110), and (111) and the hexagonal-closed-packed-Cobalt system. In a solid, the band gap is the energy difference between the conduction and valence band. When an electron in the conduction band decays to the valence band the additional energy is released either as radiation. The color of the emitted light will correspond to the energy of the band gap. Based on the value of the energy band gap (E_g) from our calculations, we could determine the wavelength of light (λ) that corresponds to the band gap energy of each system. By using the optimized geometry at PM6 and a single point calculation at HF/LANL1MB level, we found that for the Pt (100), Pt(110), and Pt(111) surfaces, the energy gaps were 3.18 (356.94 nm), 2.77 (409.78 nm), and 3.15 eV (360.34 nm), respectively. The calculation of the optical band gaps for Co-Pt(100) (Fig. 10a), Co-Pt(110) (Fig. 10b),

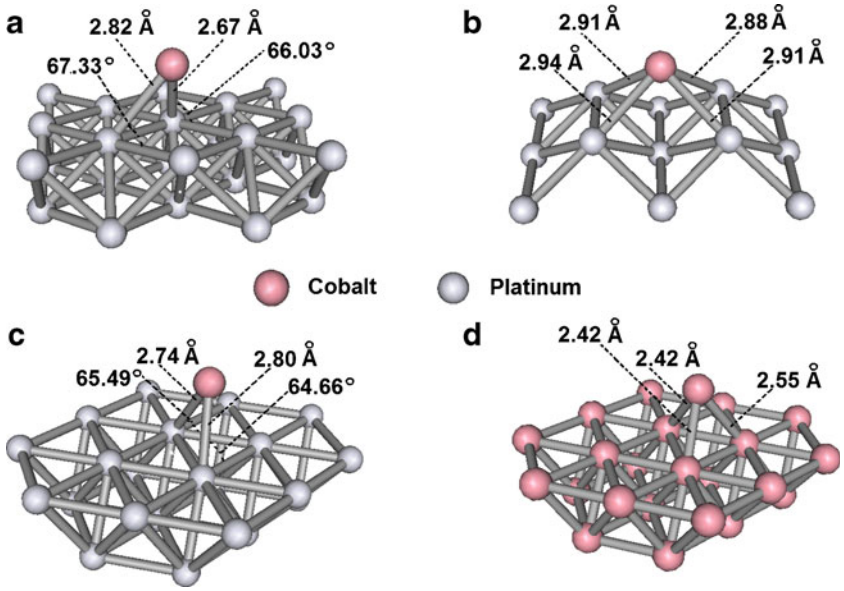

Fig. 10 Finite clusters' size models. **a** Co-Pt(100), **b** Co-Pt (110), **c** Co-Pt(111), and **d** Co-Co(0001)

and Co-Pt(111) (Fig. 10c) systems were 3.50 eV (336.97 nm) 4.42 eV (256.73 nm) and 3.46 eV (328.20 nm), respectively. A direct comparison of these values with λ where the peaks appeared in Fig. 9, indicates that peaks at 355 and 362 nm may be associated with the Pt (111) and Pt(100) surfaces, respectively. When the cobalt atom is adsorbed onto Pt(100), the λ calculated value was 337 nm which agree with the peak observed at 337 nm. This result suggests that at initial stages, cobalt upd starts on a Pt(100) surface. Observe that for Co-Pt(111) the calculated λ (328.20 nm) value compares favorably with the peak recorded at 328 nm. It is interesting to note that neither the Pt(110) surface nor the Co-Pt(110) system were detected in the spectra showed in Fig. 9. Last results suggest that for electrodepostion potentials above −0.550 V, the cobalt submonolayers are mainly favored on Pt(100) and Pt(111) surfaces. Also, it is possible to observe that the peaks recorded at 342 and 383 nm may be related with an ion adsorption on the polycrystalline platinum. A similar study to the depicted by Fig. 10 was performed substituting the cobalt atom, by Cl^-, O^{2-}, H^+ ions. The band gaps obtained for Cl^- and H^+, lead bang gaps out of the range recorded at the experimental DRS. The adsorption of the O^{2-} onto the surface gave the band gaps 2.96(384 nm) and 3.29 eV(345 nm) which may correspond to Pt(100)-O and Pt(111)-O. Also, note the presence of additional peaks, which may correspond to cobalt submonolayers deposited on faces with higher Miller indexes to those considered at present study. Finally, a key factor to get in the upd process is the existence of a strong interaction of metal (M) onto a different substrate (S), among other factors [45]. Although, several theoretical methodologies have been reported to elucidate the stages involved during upd process [46–48]; as a first approximation, we consider that the strong interaction M-S indicates that the heat of formation (ΔH_f) to incorporate a cobalt atom on Pt surface must be more negative that the involved during the incorporation of cobalt atom onto Co surface. Under this premise, we calculate at PM6 level, the ΔH_f involved during the incorporation of cobalt atom onto the different surfaces showed in Fig. 10. The incorporation energies calculated for Co-Pt(100), Co-Pt(110), Co-Pt(111), and Co-Co(surface) were −432.21, −263.31, −375.29, and −137.88 Kcal mol^{-1}, respectively. It is interesting to observe that according with this incorporation energies the formation order is Co-Pt(100)>Co-Pt(111) > Co-Pt(110) > Co-Co(surface). These theoretical results suggest that for all cases the incorporation of cobalt on platinum surface is favored with respect to the cobalt surface indicating the existence of upd process of cobalt on platinum. It must be considered that the energy incorporation defined here is different to the bond energy concept. These theoretical results agreed with the UV-DRS showed in Fig. 9.

Conclusions

Cobalt electrodeposits onto platinum polycrystalline were studied in upd conditions from an aqueous solution 10^{-2} M of $CoCl_2$ and 1 M NH_4CI at pH 9.5. The voltammetric studies, DRS-UV and theoretical quantum studies indicated the existence of upd cobalt processes mainly onto the crystallographic orientations Pt(100) and Pt(111) on polycrystalline platinum. Quantum calculations at the level PM6 indicated that the energy formation order is Co-Pt(100)> Co-Pt(111) > Co-Pt(110) > Co-Co(surface).

Acknowledgments L.H.M.H. gratefully acknowledges partial support from CONACYT through the project FOMIX-CONACYT 97144 and to the Universidad Autónoma del Estado de Hidalgo. We acknowledge to professor M.E. Palomar-Pardave for useful comments. We are also grateful to the reviewers of the manuscript for valuable suggestions.

References

1. Broeder FJA, Hoving W, Bloemen PJH (1991) J Magn Magn Mater 93:562
2. Smardz L, Szymanski B, Gontarz R, Stefanski P, Barnas (1993) J Magn Magn Mater 120:239.
3. Spörl K, Weller D (1991) J Magn Magn Mater 93:379
4. Gambardella P, Rusponi S, Veronese M, Dhesi SS, Grazioli C, Dallmeyer A, Cabria I, Zeller R, Dederichs PH, Kern K, Carbone C, Brune H (2003) Science 300:1130
5. Meier F, Zhou L, Wiebe J, Wiesendanger R (2008) Science 320:82
6. Máca F, Hofer WA, Redinger (2001) J Surf Sci 844:482–485
7. Gauthier Y, Dolle P, Boudoing-Savois R, Hebestrein W, Platzgummer E, Schmid M, Varga P (1998) Surf Sci 396:137
8. Kalousek R, Schmid M, Hammerschmid A, Lundgren E, Varga P (2003) Phys Rev B 68:233401
9. Platzgummer E, Sporn M, Koller R, Schmid M, Hofer W (2000) Varga P Surf Sci 453:214
10. Varga P, Schmid M (1999) Appl Surf Sci 141:287
11. Rafaja D, Vacínová J, Valvoda V (2000) Thin Solid Films 374:10
12. Nabiyouni G (2008) Metrology Meas Systems 15:135
13. Cren T, Rusponi S, Weiss N, Epple M, Brune H (2004) J Phys Chem B 108:14685
14. Mendoza-Huizar LH, Robles J, Palomar-Pardave M (2002) J Electroanal Chem 521:95
15. Cagnon L, Gundel A, Devolder T, Morrone A, Chappert C, Schmidt JE, Allongue P (2000) Appl Surf Sci 164:22
16. Georgescu V, Georgescu M (2002) Surf Sci 507–510:507
17. Herrero E, Li J, Abruña HD (1999) Electrochim Acta 44:2385
18. Vilchenski MC, Silva GC, Benedetti AV, Sumodjo PTA (2003) Port Electrochim Acta 21:33
19. Schaltin S, Nockemann P, Thijs B, Binnemans K, Fransaera (2007) J Electrochem Solid-State Lett 10:D104
20. Nguyen Q, Wang L, Lu G (2007) Int J Nanotechnol 4:588
21. Kongstein OE, Haarberg GM, Thonstad J (2007) J Appl Electrochem 37:669
22. Palomar-Pardave M, Gonzalez I, Soto AB (1998) Arce EM J Electroanal Chem 443:125
23. Furuya N, Koide S (1989) Surf Sci 220:18
24. Rios-Reyes CH, Ponce-Rodriguez A, Romero-Romo M, Mendoza-Huizar LH (2008) Rev Mex Fis 54:104

25. Kittel C (1986) Introduction to solid state physics, 6th edn. Wiley, New York
26. Stewart JJP (2007) J Mol Mod 13:1173
27. Hay PJ, Wadt WR (1985) J Phys 82:270
28. Stewart JJP (2008) MOPAC2007 Version 8.032 L. Stewart Computational Chemistry, Colorado Springs
29. Frisch MJ, Trucks GW, Schlegel HB, Scuseria GE, Robb MA, Cheeseman JR, Montgomery JA, Vreven T, Kudin KN, Burant JC, Millam JM, Iyengar SS, Tomasi J, Barone V, Mennucci B, Cossi M, Scalmani G, Rega, Petersson GA, Nakatsuji H, Hada M, Ehara M, Toyota K, Fukuda R, Hasegawa N, Ishida M, Nakajima T, Honda Y, Kitao O, Nakai H, Klene M, Li X, Knox JE, Hratchian HP, Cross JB, Adamo C, Jaramillo J, Gomperts R, Stratmann RE, Yazyev O, Austin AJ, Cammi R, Pomelli C, Ochterski JW, Ayala PY, Morokuma K, Voth GA, Salvador P, Dannenberg JJ, Zakrzewski VG, Dapprich S, Daniels AD, Strain MC, Farkas O, Malick DK, Rabuck AD, Raghavachari K, Foresman JB, Ortiz JV, Cui Q, Baboul AG, Clifford S, Cioslowski J, Stefanov BB, Liu G, Liashenko A, Piskorz P, Komaromi I, Martin RL, Fox DJ, Keith T, Al-Laham MA, Peng CY, Nanayakkara A, Challacombe M, Gill PMW, Johnson B, Chen W, Wong MW, Gonzalez C, Pople JA (2004) Gaussian 03W Rev. C.02. Gaussian, Inc, Wallingford CT
30. Senda N (2009) Winmostar V. 3.70. Chiba Prefecture, Ichihara
31. Igarashi K, Aramata A, Taguchi S (2001) Electrochim Acta 46:1773
32. Aberdam D, Traore S (1987) Surf Sci 180:319
33. Soto AB, Arce EM, Palomar-Pardave M, Gonzalez I (1996) Electrochim Acta 41:2647
34. Grujicic D, Pesic B (2004) Electrochim Acta 49:4719
35. Pourbaix M (1974) Atlas of electrochemical equilibria in aqueous solutions, 2nd edn. NACE, Houston
36. Vaskelis A, Jagminiene A, Tamasauskaite-Tamasiunaite L (2003) Chemija 14:72
37. Berzins T, Delahay P (1953) J Am Chem Soc 75:555
38. Delahay P (1954) New instrumental methods in electrochemistry. Interscience, New York
39. Holzle MH, Retter U, Kolb DM (1994) J Electroanal Chem 371:101
40. Christy AA, Kvalheim OM, Velapold RA (1995) Vib Spectrosc 9:19
41. Bartlett PN, Baumberg JJ, Coyleb S, Abdelsalam ME (2004) Faraday Discuss 125:117
42. Motheo AJ, Gonzalez ER, Tremililliosi-Filho G, Rakotondarinibe A, Legar JM, Beden B, Lamy C (1998) J Braz Chem Soc 9:31
43. Mendoza-Huizar LH, Palomar-Pardave M, Robles J (2004) J Mol Struct THEOCHEM 679:187
44. Stewart JJP (2008) J Mol Model 14:499
45. Sudha V, Sangaranarayanan MV (2005) J Chem Sci 117:207
46. Sánchez C, Leiva E (1999) Electrochim Acta 45:691
47. Plieth W, Lorenz WJ, Staikov G (2004) J Solid State Electrochem 8:941
48. Sanchez CG, Leiva EPM, Kohanoff J (2001) Langmuir 17:2219